



Relation between fractional flow models and fractal or long-range 2-D permeability fields

Jean-Raynald de Dreuxy, Philippe Davy

► To cite this version:

Jean-Raynald de Dreuxy, Philippe Davy. Relation between fractional flow models and fractal or long-range 2-D permeability fields. Water Resources Research, 2007, 43 (4), pp.W04431. 10.1029/2006WR005236 . insu-00155107

HAL Id: insu-00155107

<https://insu.hal.science/insu-00155107>

Submitted on 4 Feb 2016

HAL is a multi-disciplinary open access archive for the deposit and dissemination of scientific research documents, whether they are published or not. The documents may come from teaching and research institutions in France or abroad, or from public or private research centers.

L'archive ouverte pluridisciplinaire **HAL**, est destinée au dépôt et à la diffusion de documents scientifiques de niveau recherche, publiés ou non, émanant des établissements d'enseignement et de recherche français ou étrangers, des laboratoires publics ou privés.

Relation between fractional flow models and fractal or long-range 2-D permeability fields

Jean-Raynald de Dreuzy¹ and Philippe Davy¹

Received 9 June 2006; revised 29 November 2006; accepted 21 December 2006; published 25 April 2007.

[1] Fractional flow models introduced by Barker (1988) have been increasingly popular as means of interpreting nonclassical drawdown curves obtained from well tests. Fractional flow models are intrinsically isotropic scaling models depending to first order on two exponents n and d_w expressing the dimension of the structure available to flow and the flow slowdown, respectively. We study the fractional flow induced either by geometrically scaling structures such as Sierpinski- and percolation-like fractal media or by hydraulically scaling media such as long-range continuous correlated media. First, percolation and Sierpinski structures have two well-separated d_w values in the range [2.6, 3] and [1.9, 2.5], respectively. The bottlenecks, characteristic of percolation, induce a more anomalous transport (larger d_w values) than the impervious zones present at all scales of Sierpinski. Second, the realization-based values of n and d_w depend both on global and on local characteristics like the fractal dimension and the permeability around the well, respectively. Finally, solving the inverse problem on anomalous transient well test responses consists in comparing the (n, d_w) realization-based values with field data. Indeed, well tests performed from a unique pumping well must be taken as realization-based results. For the site of Ploemeur (Brittany, France), from which n and d_w have been previously determined (Le Borgne et al., 2004), the only consistent model is given by the continuous multifractals. However, the values obtained from continuous multifractals cover most of the (n, d_w) plane, and realization-based results are not selective in terms of model. So this should be replaced by the comparison of (n, d_w) values averaged over different pumping well locations, which however requires a significantly larger quantity of field tests.

Citation: de Dreuzy, J.-R., and P. Davy (2007), Relation between fractional flow models and fractal or long-range 2-D permeability fields, *Water Resour. Res.*, 43, W04431, doi:10.1029/2006WR005236.

1. Introduction

[2] In the last 15 years, interest has increased in fractional flow models, both for interpreting well tests and for representing the medium heterogeneity using models specified by a very limited number of parameters (three or four parameters in practice). Fractional flow models originate from field and theoretical studies. Field data have shown nonstandard drawdown responses and, at the same time, theoretical works have postulated the existence of fractional flow models generalizing the classical one-, two-, and three-dimensional models. Fractional flow models have been found to explain some observed nonstandard drawdown responses to well tests.

[3] Neither the field nor the theoretical studies on fractional flow models provide clear indications on the underlying medium heterogeneity that produce such nonstandard behaviors. No systematic relationship between the medium

heterogeneity and the fractional flow models has been established, whether practically or theoretically. Consequently, although this class of models appears to be more efficient than others in fitting pumping tests in heterogeneous aquifers [Le Borgne et al., 2004], the absence of a physical understanding of the model parameters makes the generalization of the fitting results to a larger geological system, and even to different pumping geometries, questionable.

[4] The relationship between heterogeneity and nonstandard drawdown response for a particular media has been searched for both in the physics literature in the framework of anomalous diffusion characterization [Havlin and Ben-Avraham, 1987] and in the hydrogeology literature. However, no systematic relationship has been investigated. The heterogeneity types inducing a nonstandard flow response should include a scaling dependence of their physical properties. Starting from this argument, three types of structures can be tested based on the scaling of the geometrical structure, the scaling of the permeability structure, or both. The geometrically scaling structure corresponds to fractals, i.e., to structures displaying holes at all scales of the medium. In this paper, holes designate impervious zones. The hydraulically scaling structures correspond to continuous media with long-range correlations. This paper deals with these two cases of geometric or hydraulic structures.

¹Géosciences Rennes, UMR 6118 CNRS, Université de Rennes, Rennes, France.

[5] The remainder of this paper is organized as follows. In sections 2 and 3, we provide the theoretical and field arguments for fractional flow models. In sections 4 and 5, we give the relationship between heterogeneity and drawdown responses in several fractal media and in long-range continuous correlated media. We synthesize the largest possible number of geometrical and hydraulic exponents. These results come from both the bibliography and the transient flow simulations performed for this study. Finally, in section 6, we compare the abovementioned results with field data.

2. Theoretical Fundamentals About Fractional Flow Models

2.1. Generalized Equations and Hydraulic Exponents

[6] Fractional flow models have been theoretically proposed as a generalization of one-, two-, and three-dimensional homogeneous media in order to interpret well tests in fractured media [Barker, 1988]. Their main parameter is the flow dimension n ranging from 1 to 3. n generalizes the Euclidean dimension to which it is equal for models of integral dimension. Their equation writes:

$$S \frac{\partial h}{\partial t} = \frac{1}{r^{n-1}} \cdot \frac{\partial}{\partial r} \left(r^{n-1} \cdot K \cdot \frac{\partial h}{\partial r} \right), \quad (1)$$

with S and K the generalized storage and permeability coefficients, respectively. With the head equal to zero everywhere for $t = 0$ and to infinity at whatever t , the general solution of this equation is as follows:

$$h(r, t) = h_r(r) \cdot \Gamma \left(\frac{n}{2} - 1, \frac{t_c(r)}{t} \right), \quad (2)$$

where $h_r(r)$ is a time-independent function, Γ is the complementary incomplete gamma function and t_c scales as r^2 . Solution (2) yields for long times ($t > t_c$) a general power law or logarithmic dependence on time $h_0(t)$ of the drawdown at the well (head at the injection point). For a constant-rate pumping test, the drawdown at the well is a power law of characteristic exponent $1 - n/2$ for $n \neq 2$ ($h_0(t) \sim t^{1-n/2}$) and the classical logarithmic function of Theis [1935] for $n = 2$ ($h_0(t) \sim \ln(t)$). The characteristic exponent can take all values in the range $[-0.5, 0.5]$ and thus provides a means of interpreting a wide range of field flow tests (see section 3).

[7] Diffusion in Barker's generalized radial flow model always remains normal because the mean square radius of diffusion $R^2(t)$ scales linearly with time t . This is shown by a simple dimensional analysis of equation (1). It means that the "speed" of diffusion measured by the diffusion coefficient $D = R^2/2t$ remains constant. Barker's generalized radial flow models have been further generalized by Acuna and Yortsos [1995] referring to works by O'Shaughnessy and Procaccia [1985] to account for the anomalously slow diffusion observed in fractal media and caused by the presence of holes at all scales of the medium. The fractal dimension d_f and the anomalous diffusion d_w are both taken into account. d_w is asymptotically defined from the mean

square radius of diffusion $R^2(t)$ by [Havlin and Ben-Avraham, 1987]:

$$R^2(t) \sim D \cdot t^{2/d_w}, \quad (3)$$

where D is the generalized diffusion coefficient and d_w is equal to 2 for homogeneous media whatever the Euclidean embedding dimension and greater than 2 for anomalously slow diffusion. The simplest diffusion equation accounting for both the fractal dimension and the anomalous diffusion writes [O'Shaughnessy and Procaccia, 1985]:

$$S \frac{\partial h}{\partial t} = \frac{1}{r^{d_f-1}} \cdot \frac{\partial}{\partial r} \left(r^{d_f+1-d_w} \cdot K \cdot \frac{\partial h}{\partial r} \right), \quad (4)$$

with S and K the generalized storage and permeability coefficients, respectively. Several other equations have been later proposed, and the existence as well as the exact form of the diffusion equation remains an open question [Roman, 2004]. However, for constant-rate pumping tests, the head at the well always scales as $h_0(t) \sim t^{1-d_f/d_w}$. Compared to Barker's model, the hydraulic dimension n is related to d_w and d_f by:

$$n = 2 \cdot \frac{d_f}{d_w}. \quad (5)$$

[8] In a normal diffusion ($d_w = 2$), n is equal to d_f , so n has often been mistaken for the fractal dimension. In fact, because n is proportional to d_f (5), a denser medium having a larger fractal dimension d_f has a larger flow dimension. However, n is also inversely proportional to d_w , showing that the slowdown of diffusion due to a lack of connectivity reduces the flow dimension. As n and d_w are scaling exponents, it is implicitly assumed that the scalings of $R^2(t)$ and $h_0(t)$ are consistent over several orders of magnitude. This should not be confused with a medium undergoing a transition of dimension at a given scale [Barker, 1988]. Such transition models have especially been proposed for fractured media. The flow dimension increases from 1 to 3 when flow is localized around the well in one-dimensional structures, farther from the well in two-dimensional planes and possibly in full three-dimensional networks at larger scales. When drawdown is observed over a limited time range, the transition of dimension can be mistaken for the nonintegral flow dimension.

2.2. Relationship Between Exponents

[9] There is a full analogy between the classical flow equation and the diffusion equation as long as the relationship between hydraulic head and flow remains linear [Havlin and Ben-Avraham, 1987]. The diffusion equation governs the probability $P(r, t)$ of finding a diffusing particle at time t and position r . Its counterpart in the flow equation is the head $h(r, t)$. Practically, the pulse test gives a good example to express this analogy. Performing a pulse test at a given well is analogous to injecting a pulse of particles at the initial time at the well position. The counterpart of the drawdown at the well $h_0(t)$ in the physics of diffusion is the probability for a particle to return to its injection position at time t .

[10] The analogy between flow and diffusion equations leads to a relationship between the diffusion and the hydraulic conductivity known as the relation of Einstein [Havlin and Ben-Avraham, 1987]. In electric terms, the

conductivity σ is proportional to the apparent diffusivity $D_{\text{app}}(R) = R^2/t$ multiplied by the density of charge carrier n :

$$\sigma \sim n \cdot D_{\text{app}}. \quad (6)$$

From the analogy between electricity and fluid mechanics, σ is equivalent to K and n is equivalent to the density of the support. These quantities scale with length R as $K(R) \sim R^{-\tilde{\mu}}$, $D_{\text{app}}(R) = R^{2-d_w}$, and $n(R) \sim R^{d_f-d}$, where $\tilde{\mu}$ is the exponent of the permeability scaling and d is the embedding Euclidean dimension. Equation (6) leads to the following relationship between the two hydraulic exponents $\tilde{\mu}$ and d_w :

$$d_w = 2 - d + d_f + \tilde{\mu}. \quad (7)$$

[11] The transient exponent (more typically called anomalous diffusion exponent) d_w can be theoretically derived from the steady state exponent $\tilde{\mu}$. While hydraulic exponents can be universally interrelated by equation (7), there is no general way of getting the hydraulic exponents from the geometrical exponents [Stauffer and Aharony, 1992]. Such a relationship was the object of the conjecture of *Alexander and Orbach* [1982]. It hypothesized that the so-called spectral dimension d_s (equal to n in equation (5)) is an invariant for fractals:

$$d_s = n = 2 \frac{d_f}{d_w} = \frac{4}{3} \quad (8)$$

[12] Numerical simulations on the Sierpinski gasket and on percolation clusters first supported this conjecture and later discarded it [Grassberger, 1999]. However, it explains that n values are clustered around 4/3 for a broad range of two-dimensional systems including percolation clusters and Sierpinski gaskets.

3. Field Relevance of Fractional Flow Models

3.1. Practical Determination of n and d_w

[13] $h_0(t)$ and $R^2(t)$ can be practically determined from field tests as it was done with the crystalline aquifer in Ploemeur (France) [Le Borgne et al., 2004]. $h_0(t)$ is directly the head variation at the injection well. $R^2(t)$ is more difficult to obtain because it supposes the knowledge of the diffusion front in the medium. It can, however, be derived from the drawdown observation at several points. Fitting the drawdown at a piezometer at a distance r from the injection well with function (2) yields a characteristic time $t_c(r)$, which is the reciprocal function of $R^2(t)$. As a result, t_c scales as the square of r in Barker's model and generalizes to $t_c(r) \sim r^{d_w}$ with anomalous diffusion. The scaling of t_c as a function of r is best determined when the drawdown has been observed over the widest possible range of distances from the well. The piezometer network should cover the widest possible range of distances from the well. Fitting $t_c(r)$ against r in a bi-logarithmic graph gives d_w . For sufficiently long well tests, $h_0(t)$ and $t_c(r)$ are defined over orders of magnitude, and provided that $h_0(t)$ and $t_c(r)$ are consistent power laws, their exponents are equal to $-n/2$ and d_w , respectively.

3.2. A Review of n Exponents Provided by Field Well Tests

[14] The Generalized Radial Flow model has been most generally assessed on drawdowns at the well and at distant

piezometers but without determination of $t_c(r)$. This kind of analysis leads to the generalized flow dimension n . The n value gives a first indication of the relevance of fractional flow models. Characteristic n values in tested fields are summed up in Table 1. Exponent n is consistently determined over 1 to 3.7 orders of magnitude and ranges from 0.2 to 2.5. Most of the exponents larger than 2 are obtained from packer tests in intervals ranging from 2 to 10 m and for restricted investigation times (less than 24 h) [Kuusela-Lahtinen et al., 2003]. In such tests, the active well interval is punctual (zero-dimensional) with respect to the three-dimensional medium. The test yields a sampling at early time of a space of dimensions 2 to 3 corresponding to a space between a plane and a volume. For fields where several piezometers have been observed, values of the flow dimension n are more often clustered around a given value [Acuna et al., 1992; Hamm and Bidaux, 1996; Le Borgne et al., 2004; Leveinen, 2000] than dispersed [Acuna et al., 1992; Bangoy et al., 1992]. In the study of Bangoy et al. [1992], the time range is the smallest and may not be wide enough to get consistent tendencies leading to dispersed n values. In the tests reported from the Geysers geothermal field by Acuna et al. [1992], values of n are obtained in three different wells contrary to the other reported tests, for which values are obtained from different piezometers. For tests performed from a given full well and that are long enough to yield consistent power law drawdown signals, values of n obtained in the well and in the distant piezometers are clustered around a given value. The dimension n ranges between 0.94 and 2.32 with most of the values between 1.4 and 1.75. As expected when pumping in the whole well and except for the 2.32 value, all n values are lower than 2. Finally, the table does not show any difference between sedimentary and crystalline rocks. The dimension could be more influenced by the nature, density, and organization of fractures that require more geophysical characterization.

3.3. Exponent d_w in the Ploemeur Site

[15] Exponent d_w is more difficult to derive as it requires the existence of piezometer drawdowns at different distances from the pumped wells. This experiment has been completed in the field site of Ploemeur (Brittany, France) where piezometers are gradually disposed from 4 to 300 m from the pumped well [Le Borgne et al., 2004]. Results show that the anomalous diffusion exponent d_w is significantly larger than 2 and contained in the interval [2.5, 3.8] with a most probable value at 2.8, depending on the fitted n value.

[16] These results obtained in different sites show first that the classical homogeneous two-dimensional interpretation of Theis [1935] for which $n = 2$ and $d_w = 2$ fails to fit the previously mentioned data. Second, $h_0(t)$ and $t_c(r)$ are consistent power laws of which exponents lead to n and d_w characterizing the time evolution of the drawdown and the diffusion rate of the well test-induced perturbation.

4. Flow and Anomalous Diffusion Exponents n and d_w in Fractal Media

[17] Among the wide spectra of existing fractals, the most commonly used for porous media are Sierpinski- and percolation-like structures [Acuna and Yortsos, 1995; Berkowitz and Balberg, 1993]. We have used both numerical simulations and results from the bibliography

Table 1. Power Law Exponents n Determined in Different Sites From Time Chronicles of Duration Varying From 1.7 to 3.7 Orders of Magnitude

Localization	Geology	Interpretation Duration Range	Number of Orders of Magnitude	n	Reference
“Fractured Reservoir in Western Venezuela”		[1 hr, 150 hr]	2.15	1.38	[Acuna <i>et al.</i> , 1992]
“Geysers Geothermal Field”	Shear zone in a graywacke reservoir rock	[7 min, $5 \cdot 10^2$ min] [10 min, $5 \cdot 10^4$ min] [10 min, 10^4 min] [0.2 hr, 50 hr]	1.85 3.7 3 2.4	1.2 1.7 2.32 1.72	
“Naturally Fractured Reservoirs”					
“Monterey Formation”	Fractures in brecciated chert and dolomite	[2, 200] (normalized time)	2	0.94	
Pocheon (South Korea)	Biotite granite and granitic gneiss of Precambrian age	[0.3 hr, 24 hr]	1.9	1.45	[Hamm and Bidaux, 1996]
Ploemeur (Brittany, France)	Densely fractured pegmatite at the contact between granite and micaschist	[0.1 hr, 10^2 hr] [1 hr, 10^3 hr]	3	1.6	[Le Borgne <i>et al.</i> , 2004]
Leppävirta (South-Central Finland)	Fracture zone in a magmatic gneiss	[0.5 hr, 10 hr]	~ 1.3	1.45–1.5	[Leveinen, 2000]
Romuvaara (Finland) ^a	Low-conductivity crystalline rock	[0.1 hr, 1 hr]	1	< 2 (10%) 2 (50%) 2–2.5 (40%)	[Kuusela-Lahtinen <i>et al.</i> , 2003]
Pyrenean Granite	Hercynian granitic basement composed of granodiorites and monzogranites	[1 hr, 25 hr]	1 to 2	0.76, 1.26, 1.40, 1.34, 1.36	[Bangoy <i>et al.</i> , 1992]
Southern France Carbonate Aquifer	Subhorizontal joints in which significant karstification has been observed	[0.01 hr, 1 hr]	1 to 2	0.2, 0.5, 0.58, 0.62, 0.76, 0.9, 1.04, 1.14	[Bangoy <i>et al.</i> , 1992]
Bloemfontein (South Africa)	Fractured mudstones and sandstones	[2 min, $5 \cdot 10^2$ min] [10 min, $9 \cdot 10^2$ min]	1.7 1.95	1.75 1.85	[Riemann <i>et al.</i> , 2002]

^aTests were preformed between packers leaving a 2-m and 10-m open tested zone.

to synthesize the largest possible number of geometrical and hydraulic exponents (results are synthesized in (Table 2)). When numerical simulations are necessary, the fractal dimension is determined by the box counting method [Feder, 1988]. The hydraulic dimensions n and d_w are determined by simulating transient flow with an injection point at the grid center and constant heads on the borders. A head pulse is imposed at the initial time. The flow equation is discretized with a finite volume scheme integrated in the time domain with a backward differentiation method, i.e., a multistep scheme in time [Hindmarsh, 1983]. The anomalous diffusion exponent d_w is deduced from the power law fit of the square radius of diffusion $R^2(t)$ of the drawdown. The hydraulic dimension is the power law exponent derived from the power law fit of the drawdown at the injection point. Fits are taken in a well-bounded time range from the exit time of the injection link to the exit time of the system. The exit time of the injection link is the time at which the mean radius of diffusion $\sqrt{R^2(t)}$ is equal to the scale of the mesh link that contains the well. The exit time of the system is the time at which 1% of the injected flow has crossed the borders. In practice, it means that signals are fitted after diffusion has left the link of the well and before diffusion has reached the system borders. The system size is generally taken as $4^4 = 256$ or $3^5 = 243$. First, we validate the numerical method on annular media. We check that the scale-dependent permeability $K(r) \sim r^{-\theta}$ induces an anomalous diffusion exponent $d_w = 2 + \theta$ whatever θ in $[-0.5, 1.0]$. Second, we validate the numerical procedures on classical percolation and on the Sierpinski gasket. For the classical off lattice infinite cluster at percolation threshold and $L = 50$ (Figure 5a), we find numerically $d_w = 2.96$ instead of $d_w = 2.86$ over 50 realizations

and $n = 1.3$ as expected. For the Sierpinski gasket (Figure 1b), we find the expected value of the exponents with a precision of 0.05 for a size of 256.

4.1. Sierpinski Structures

4.1.1. Sierpinski Definition and Generation

[18] The first type of complex objects that we explore are derived from Sierpinski, whose main feature is the presence of holes at all scales of the medium. The classical Sierpinski is the Sierpinski gasket. Its construction relies on triangle patterns. At the first construction stage, a solid equilateral triangle is divided into four smaller triangles, from which the middle triangle is removed (the gray pattern in Figure 1a shows the outcome of the first generation step). This algorithm is repeated iteratively through scales. At each stage, the middle triangle of the remaining triangles is removed. Figure 1a is the result of generation at the sixth iteration. All structural and hydraulic exponents can be analytically calculated [Havlin and Ben-Avraham, 1987]: $d_f = \ln(3)/\ln(2) \sim 1.585$, $d_w = \ln(5)/\ln(2) \sim 2.322$, and $n = 2 \cdot \ln(3)/\ln(5) \sim 1.365$. Relation (5) between n , d_w , and d_f is verified and n is close to $4/3$ of the conjecture of Alexander and Orbach. The same generation principle can be applied to a square pattern, where one of the four smaller squares is removed and the process is iterated through scales (Figure 1b). Exponents are equal to those of the Sierpinski gasket, showing that the exponents are not sensitive to the details of the pattern but to the scale invariant, which is the number of divisions n_{div} .

[19] Based on the principle of keeping a constant rate of voids through scales, the Sierpinski gasket can be extended to what we call the “generalized Sierpinski” (Figure 1c).

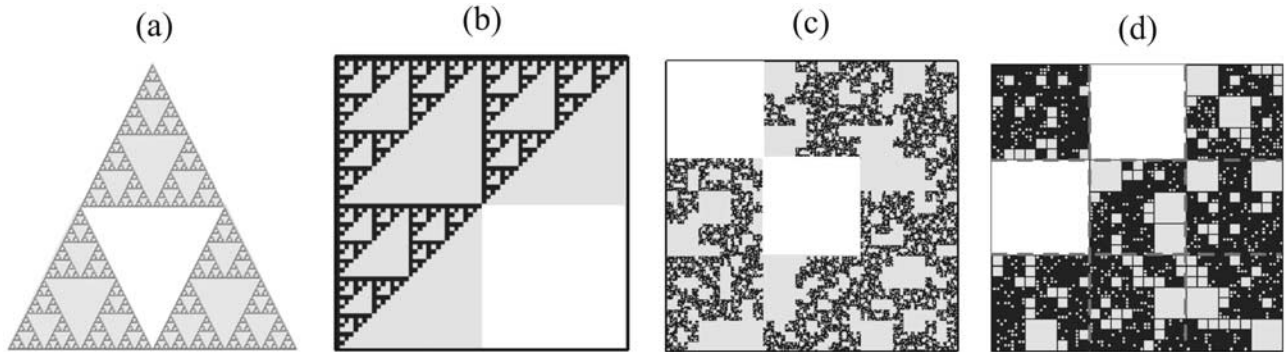


Figure 1. Examples of Sierpinski structures. (a) Classical two-dimensional Sierpinski gaskets. (b) Generalized Sierpinski corresponding to the Sierpinski gasket (Figure 1a). (c) Generalized Sierpinski. (d) Sierpinski lattice. Figures 1c and 1d were both generated with a 9-square pattern ($n_{\text{div}} = 3$) and an occupation probability of 0.8. Fractal dimension d_f is 1.8 and 1.9 for Figures 1c and 1d, respectively. Gray color is the superimposition of the outcome of the first step of the recursive generation.

The initial square is divided into n_{div}^2 smaller squares out of which a proportion p is retained and $(1 - p)$ is removed. Figure 1c is the result of a five-step generation process with a division into $n_{\text{div}}^2 = 3^2$ smaller squares and a proportion of retained squares $p = 7/9$. As opposed to the Sierpinski pattern in Figure 1b, the initial pattern is not exactly replicated through scales, as the removed squares are chosen randomly in each larger square. The main issue of the generalized Sierpinskis is that they become disconnected as the number of generation steps increases. In the example of Figure 1c, after the first generation step (gray pattern), both the right and left borders and the bottom and top borders of the structure are connected. However, after the fifth generation step (solid black pattern), no connected path between the right and left borders and between the bottom and top borders can be observed (diagonal neighboring meshes being disconnected). On average, the probability of connection for $p = 0.8$ and $n_{\text{div}} = 3$ decreases from 0.46 to 0.27 for a number of generation steps increasing from 3 to 5. Even by imposing a low permeability to their void space, the transient response of the disconnected Sierpinskis still remains normal, being dom-

inated by these critical flow regions of low permeability. As a result, only the connected generalized Sierpinskis are retained among all the generated ones. Such connected structures are obtained with a small void probability $(1 - p)$ and with a restricted number of generation steps. In practice, $p \geq 0.6$ and the system size is around 250.

[20] To ensure connectivity, the “generalized Sierpinskis” are transformed into Sierpinski lattices (Figure 1d) [Doughty and Karasaki, 2002]. The fundamental pattern of a Sierpinski lattice is the pattern of a generalized Sierpinski with additional vertical and horizontal fully crossing links. These links are placed at the border of the smaller squares and are underlined by the dark gray dashed line in Figure 1d. Whatever the probability of occupation and the number of iterations, the four edges of the structure are connected. At this point, two issues should be addressed. First, the pattern is not necessarily connected between the grid border and the grid center, which will be used for the injection point. Second, even after several generation steps, the structure keeps a high degree of central symmetry around the grid center. To solve these issues, the studied system of size L is extracted from a larger Sierpinski lattice of size $n_{\text{div}} \cdot L$.

Table 2. Exponents n and d_w for Different Models

Medium Type	Details	d_f	d_w	n	Reference
Homogeneous		2	2	2	[Theis, 1935]
Barker		?	2	$1 \leq n \leq 3$	[Barker, 1988]
Sierpinski	Gasket	1.585	2.322	1.365	[O'Shaughnessy and Procaccia, 1985]
	Generalized	[1.55, 2]	[2, 2.45]	[1, 2]	This study
	Lattice	[1, 2]	[1.9, 2.5]	[1, 2]	This study
Percolation	Cluster at threshold	1.896	2.878	1.318	[Grassberger, 1999; Porto et al., 1997]
Continuum Percolation (Cluster at Threshold)	Backbone at threshold $p(K) \sim K^{-\alpha}$ with $0 < \alpha < 1$	1.643 1.896	2.626 1.896 + 0.75 · max(1.3, 1/(1 - α))	1.251 [1.318, 0]	[Grassberger, 1999] [Kogut and Straley, 1979; Matcha et al., 1986; Stenull and Janssen, 2001]
Correlated Percolation at Threshold	$\langle K(r)K(r + R) \rangle \sim R^{-a}$ $0 \leq a \leq 2$	1.896	[2.29, 2.878]	[1.25, 1.66]	[Prakash et al., 1992]
	$\langle K(r)K(r + R) \rangle \sim R^H$ $0 \leq H \leq 1$	1.896	[2.73, 2.878]	[1.251, 1.39]	[Sahimi, 1996]
Fractional Brownian Motion	Performed on $\ln K$ $0 < H < 0.5$	2	[2, 2.45]	?	[Saadatfar and Sahimi, 2002]
Continuous Multifractals	$\langle K(r)K(r + R) \rangle \sim R^{-a}$ $0 \leq a \leq 1$	2	[1.5, 2.75]	[1.5, 2.75]	[de Dreuzy et al., 2004]

Practically, the extracted domain is centered on the injection point randomly chosen on the structure in the larger domain. The injection point is drawn uniformly in the centered square of size L of the larger domain.

[21] Both generalized Sierpinski lattices and Sierpinski lattices are parameterized by the probability of occupation $p \in [0, 1]$ and the number of divisions n_{div} . Practically, the initial square is divided into 4, 9, or 16 smaller squares ($n_{\text{div}} \in [2, 4]$). We define the system size L as the ratio of the domain size to the resolution scale. L is directly linked to the number of generation steps by $L = m_{\text{div}}^g$, where g is the number of generation steps. In the simulations, $L = 243$ or 256 as previously stated.

4.1.2. Fractal Dimension

[22] For the generalized Sierpinski lattices, the fractal dimension d_f characterizes the increase in mass M as a function of scale L such as $M \sim L^{d_f}$. As rescaling of the system size by a factor of n_{div} induces a rescaling of mass by a factor of $p \cdot n_{\text{div}}^d$, the fractal dimension is as follows:

$$d_f = \frac{\ln(p \cdot n_{\text{div}}^2)}{\ln(n_{\text{div}})} = 2 + \frac{\ln(p)}{\ln(n_{\text{div}})}. \quad (9)$$

[23] We validated this analytical result by numerical simulations whatever n_{div} and p . For $n_{\text{div}} = 4$, Figure 2 shows a good agreement between analytical and theoretical results. The connected generalized Sierpinski lattices (stars in Figure 2) have, on average, a smaller fractal dimension. In fact, connectivity forces the mass to concentrate around more linear structures of smaller fractal dimension. On the contrary, Sierpinski lattices have, on average, larger fractal dimensions because of the addition of links to the generalized Sierpinski lattices. The fractal dimension of the structure for $n_{\text{div}} = 4$ does not converge to 1 but to 1.15 when p tends to zero because the structure is not a simple crossing line but three equally spaced horizontal and vertical lines. The entropy and correlation dimensions corresponding to the second- and third-order dimensions of the structure give identical results as the fractal dimension, thus supporting the intuitive assessment that the structure is a pure fractal. We note that the difference in fractal dimensions between the Sierpinski lattices and the analytical result of equation (9) is significant and larger than the difference observed by *Doughty and Karasaki* [2002].

4.1.3. Flow and Anomalous Diffusion Exponents

n and d_w

[24] We simulate pulse tests in the connected generalized Sierpinski lattices and the Sierpinski lattices, which consists in a head pulse injected at the initial time. Examples from a single realization of square radius of diffusion $R^2(t)$ (Figures 3a and 3b) and drawdown at the injection point $h_0(t)$ (Figures 3c and 3d) are compared with the evolution of the structure's mass $M(r)$ (Figures 3e and 3f). $M(r)$ is obtained by counting the number of occupied meshes in a shell of radius r . It scales statistically as $M(r) \sim r^{d_f-1}$ for a structure of dimension d_f . The power law exponents of $R^2(t)$ and $h_0(t)$, $2/d_w$ and $-n/2$, respectively, are given by the scales on the right of Figures 3a, 3b and 3c, 3d. They display large variations of 0.2 and 0.5 units, respectively. These variations are partly correlated with the evolution of $M(r)$. For example, the increase in the slope of $h_0(t)$ for the Sierpinski lattice of $d_f = 1.78$ (squares and solid curves in Figure 3c)

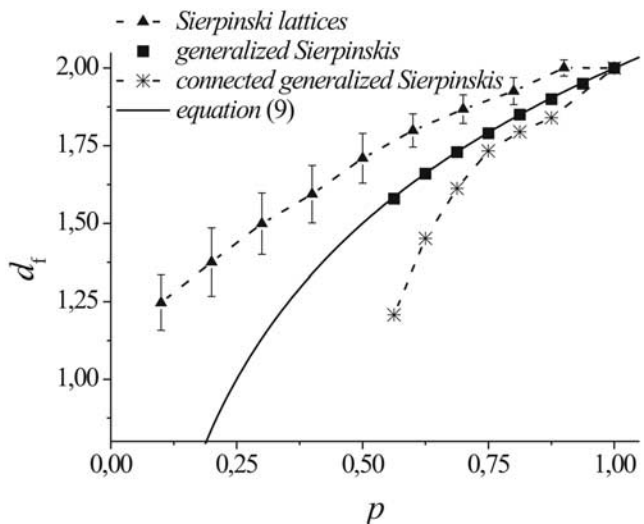


Figure 2. Fractal dimensions d_f for the generalized Sierpinski lattices, connected generalized Sierpinski lattices, and Sierpinski lattices. These structures were generated with $n_{\text{div}} = 4$, $g = 4$, and $L = 256$. Error bars for the Sierpinski lattices have been obtained from 100 realizations. Fractal dimensions have been computed by the box counting method.

can be interpreted as an increase in structure dimensionality consistent with the slope increase of $M(r)$ (Figure 3e). Still, the evolution of $M(r)$ does not explain all the variations of $R^2(t)$ and $h_0(t)$ exponents. On the contrary, for the generalized Sierpinski (black stars and curves of Figures 3b and 3d), the power law slope of $M(r)$ in Figure 3f is roughly constant, whereas the exponents of $R^2(t)$ and $h_0(t)$ still vary, probably because of a lack of connectivity. This is consistent with the evidence that $M(r)$ does not capture connectivity effects, and thus cannot explain all the hydraulic exponent variability. Although locally large, the exponent variations do not show systematic tendencies nor trivial changes in dimension like a transition of dimension between one and two [Barker, 1988]. On the contrary, linear fits performed over the whole time range give good approximations of $R^2(t)$ and $h_0(t)$ (Figures 3a–3d). Similar oscillations are also observed in Sierpinski carpets and are attributed to the existence of holes within the medium acting as “internal boundaries” [Sellers and Barker, 2005]. As particles move away from the boundaries, they speed up until they are influenced by another internal boundary.

[25] According to this methodology, we systematically determine exponents n and d_w on each realization of connected generalized Sierpinski and Sierpinski lattices for different values of the occupation probability p (Figure 4). n and d_w do not depend on the system size. We check with $n_{\text{div}} = 2$ that the mean and distribution of n and d_w are similar for the system sizes $L = 128$ and $L = 256$.

[26] For the connected generalized Sierpinski, d_w and n evolve monotonously with d_f in a similar way whatever n_{div} . A decrease in fractal dimension d_f induces a nearly linear increase in d_w and decrease in n such as $d_w = 4 - d_f \pm 0.1$ and $n = 2 \cdot (d_f - 2) \pm 0.1$ for $d_f \in [1.6, 2]$. We also find a large standard deviation of 0.2 of the exponents around their mean value. A similar variability is obtained for Sierpinski carpets, for which the generation pattern is kept unchanged

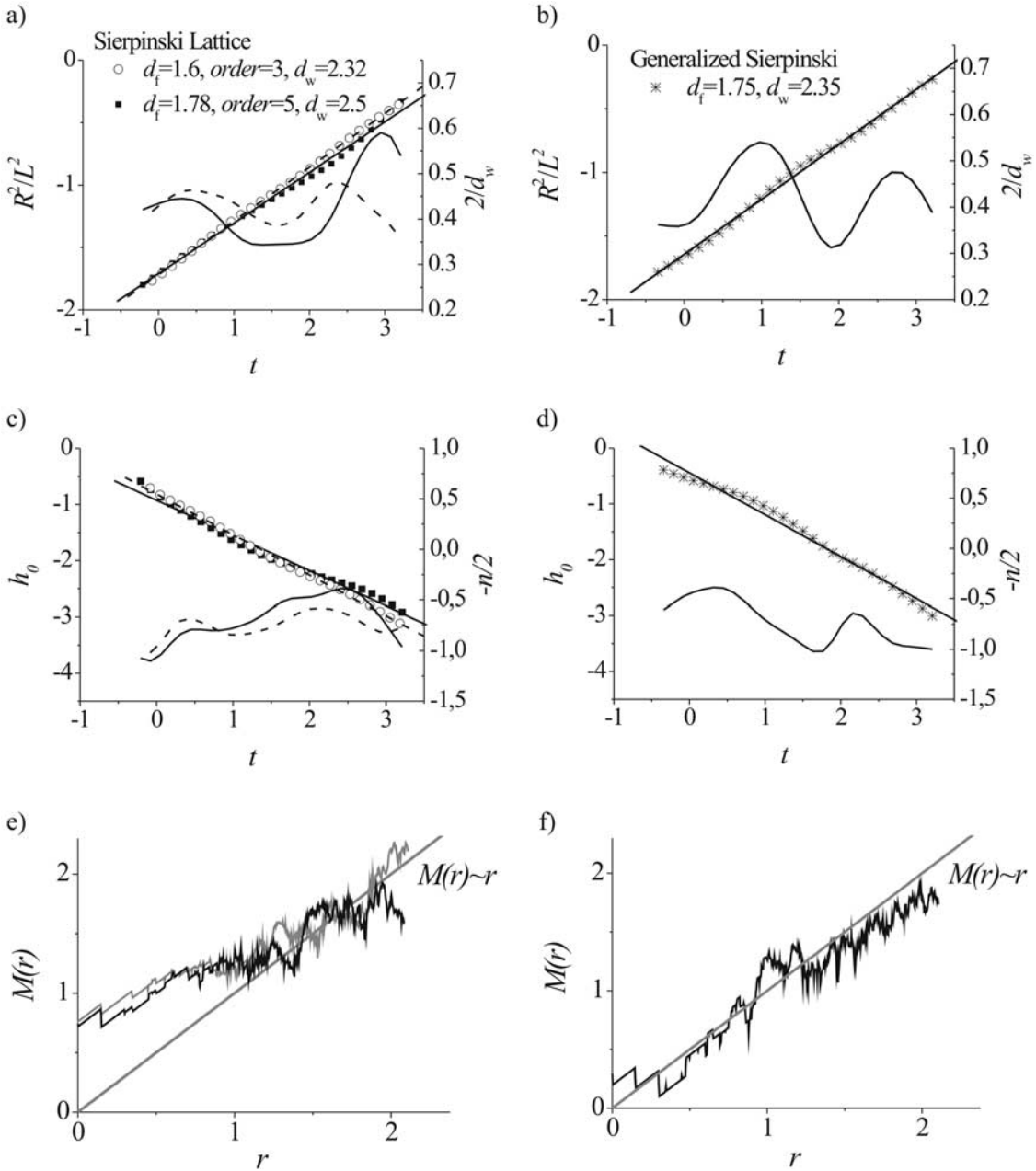


Figure 3. Examples of $R^2(t)$ normalized by the system size L (a and b), $h_0(t)$ in bi-logarithmic graphs (c and d) and the mass evolution $M(r)$ as a function of the distance from the well r (e and f) for two Sierpinski lattices (a, c, e) and one generalized Sierpinski (b, d, f). The derivatives of the curve are also shown and measured by the scale on the right.

at each generation scale [Dasgupta *et al.*, 1999], as opposed to the generalized Sierpinski for which the generation pattern is modified through scale (Figure 1c). The drawback of the Sierpinski carpets is their high degree of regularity stemming from the repetition of the same identical pattern at each generation scale. For the Sierpinski carpets, the anomalous diffusion exponent ranges from a lower bound given by Kim *et al.* [1993] to the value obtained for loopless structures $1 + d_f$ [Havlin and Ben-Avraham, 1987]. An example of Sierpinski carpet generated with $n_{\text{div}} = 7$ and $p = 30/49$ corresponding to $d_f = 2.748$ gives indeed d_w dimensions in the interval [2.194, 2.746] [Dasgupta *et al.*, 1999].

[27] For the Sierpinski lattices, the anomalous diffusion exponent d_w and the hydraulic dimension n depend both on the fractal dimension and on the order of the link on which lies the injection point (orders are identified by numbers or letters in Figures 4c and 4d). The order of a link identifies the step of the cascade process at which a link is generated. The order o of a link is related to its length l by:

$$o = 1 + \frac{\log(L/l)}{\log(n_{\text{div}})}, \quad (10)$$

where L is the system size. Orders range from 1 for links that cross the whole ($l = L$) system to $n_{\text{div}} + 1$ for the

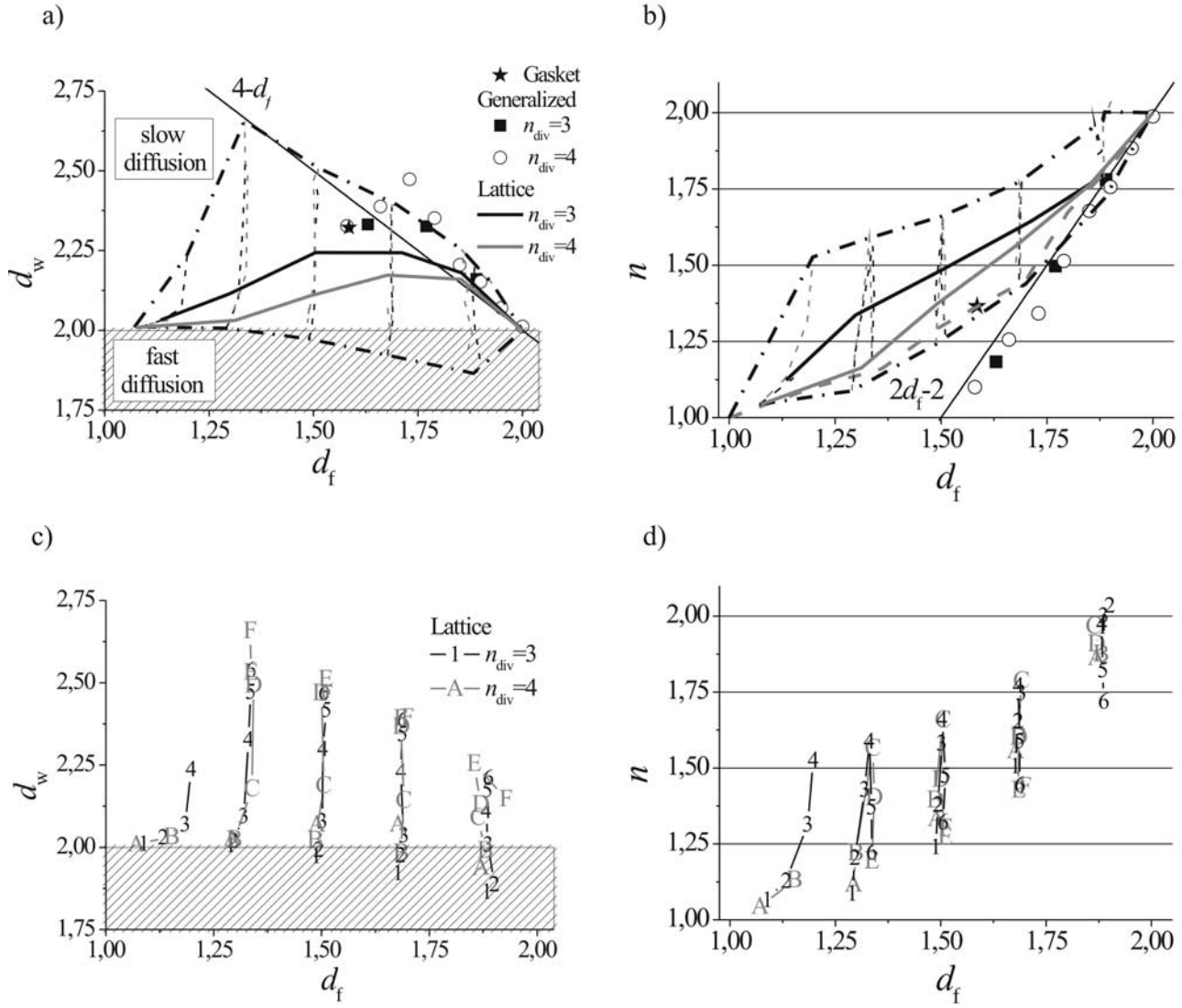


Figure 4. Anomalous diffusion and hydraulic exponents d_w and n for the generalized Sierpinski (solid symbols) and for the Sierpinski lattices. Solid lines are averages over all realizations whatever the order, whereas points identified by numbers stand for given orders of the injection point. These results were established from a total of 40,000 realizations.

smallest links. The anomalous diffusion exponent d_w increases when the fractal dimension decreases for $1.25 < d_f \leq 2$ (Figure 4a) as well as when the order increases (Figure 4c). Hydraulic dimensions n are clustered around the mean tendency $n = d_f$ and display a maximum for orders 3 or 4 (Figure 4d). For the Sierpinski lattices, the results of *Doughty and Karasaki* [2002] (dashed gray curve in Figure 4b) are almost exactly equal to the one we have found for the Sierpinski lattices generated with the injection point on a first-order link. We note that the number of divisions n_{div} is a parameter of secondary importance as both d_w and n take close values for n_{div} equal to 3 and 4.

[28] Introducing the order o leads to a more precise characterization of exponents n and d_w rendered by a decrease in their variability roughly by a factor of 2. Expressed as d_f and o , d_w and n variabilities are, on average, around 0.15 and 0.1.

[29] Both for generalized Sierpinski and Sierpinski lattices, the smaller the fractal dimension, the more anomalous

the diffusion due to the increasing proportion of holes. For Sierpinski lattices, when the fractal dimension is lower than 1.25, structures become almost linear leading to a normal diffusion identified by the trivial dimension $d_w = 2$. For Sierpinski lattices, the nature of diffusion is also controlled by the order of the injection link: the higher the order, the more anomalous the diffusion. To interpret this result, we first notice that the diffusing drawdown generally goes through links of decreasing orders to reach the borders. If the fluid is injected in a low-order link, the diffusing drawdown remains in the network of low-order links, which forms a quasi-regular grid. The diffusion scaling is thus not supposed to depart from the normal diffusion model with $d_w = 2$. Now if the fluid is injected in a high-order link, the diffusing drawdown will explore a complex system ranging from the high-order injection link to the low-order links that reach boundaries. The diffusion is slowed down by this complex geometry and we obtain the abnormal diffusion exponent $d_w > 2$, as expected.

[30] Note that relation (5) between n , d_f , and d_w is verified neither on the mean exponents nor on the exponents taken individually. We suspect that this discrepancy results from local effects around the injection points that are taken into account in d_w and n , but not in d_f that is an average measurement. Instead of d_f , we use a local measurement, which is the power law exponent d_N of the structure density $M(r)$ counted on shells of evolving radii centered on the injection point. By replacing d_f by d_N in equation (5), we find a much better relation between n and d_w , such as

$$n = (0.9 \pm 0.1) \cdot \frac{2d_N}{d_w}. \quad (11)$$

From this relation, n is directly proportional to d_N and the maximum of the hydraulic dimension n for orders 3 or 4 results from the existence of a maximum for d_N . Qualitatively, for intermediary orders around 3–4, the average d_N value is maximum because the structure close to the injection point is similar to the structure away from it. For other orders, the structure close to the injection point is either sparser or denser, inducing at some point a drop in the scaling increase. Interpreting n as the dimension of the hydraulically accessible space, n is larger than the fractal dimension for intermediate orders 3 to 4 and lower for extreme orders.

[31] These results show that the hydraulic exponents n and d_w depend on a global as well as on a local characteristic, i.e., the fractal dimension d_f , and the order o , respectively. Both characteristics are important. Should the order be ignored, the exponents averaged over all simulations (black and red lines in Figure 4) do not give a good description of the exponent variability as displayed when accounting for the order of the injection link (numbers and letters in Figure 4).

4.2. Percolation-Type Structures

[32] The second type of complex objects that we explore is percolation-type clusters, whose scaling properties are well known. Percolation has often been chosen as a framework for studies of flow in heterogeneous media [Berkowitz and Balberg, 1993]. For a system of small sticks, the percolation threshold is classically reached by randomly adding sticks until the connection between a set of predefined geometrical borders is achieved. The connecting structure, called the infinite cluster, is a fractal of dimension $d_f = 91/48 \sim 1.896$ in two dimensions [Stauffer and Aharony, 1992] (Figure 5a). The major part of the infinite cluster is contained in the dead ends, defined as the part of the structure that cannot carry any fluid. Removing the dangling ends from the infinite cluster leads to the backbone, which is also a fractal of smaller dimension $d_{fb} = 1.643$. The backbone is made up of a succession of red links and blobs (Figure 5b). If one of the red links is removed, the system becomes disconnected. The number of red links n_{rl} scales as $n_{rl} \sim L^{-0.75}$. Both the infinite cluster and the backbone at threshold are interesting because they are well-defined fractals of precisely characterized internal structure. The hydraulic exponents n and d_w are consistently derived either directly or from Einstein's relation (7) for both the infinite cluster and the backbone. For the infinite cluster $d_w = 2.878$ and $n = 1.318$, and for the backbone $d_w = 2.626$ and $n = 1.251$.

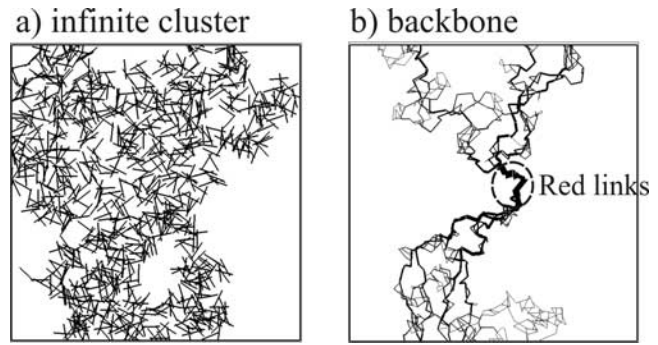


Figure 5. Infinite cluster and backbone at percolation threshold. The backbone was obtained by imposing impervious conditions to the vertical system sides. The line thickness of the backbone links is a function of a vertically imposed head gradient.

[33] From this classical structure, percolation has been extended independently in two directions, to account first for sticks of different permeabilities and then for correlations between sticks. These two extensions are called continuum percolation and correlated percolation, respectively. Continuum percolation structures are obtained first by generating a classical infinite cluster at threshold and thereafter by imposing a permeability to each stick drawn in a power law distribution such as $p(K) \sim K^{-\alpha}$ where $0 < \alpha < 1$. The fractal dimension remains that of the infinite cluster of classical percolation $d_f \sim 1.896$. The permeability scaling exponent $\tilde{\mu}$ is consistently determined by variation calculus [Kogut and Straley, 1979], by decomposition on the Links and Nodes model [Matcha et al., 1986], and by renormalization group analysis [Stenull and Janssen, 2001]. It leads from Einstein's relation (7) to $d_w = \max(2.878, 1.896 + 1/[1.33 \cdot (1 - \alpha)])$. n can be obtained directly from equation (5). Thus, for α values smaller than $\alpha_c = 0.23$, transport exponents are equal to those of the classical percolation infinite cluster. Concerning α values larger than α_c , the larger the α value, the greater the probability of generating low-permeability links. The latter create in the system more bottlenecks, thus inducing higher values of the anomalous diffusion exponent d_w .

[34] Correlated percolation systems are obtained with long-range correlations of the site occupation probability such as $C(R) = \langle K(r) \cdot K(r + R) \rangle = f(\lambda) \cdot R^{-(2 - \lambda)}$ with $0 \leq \lambda \leq 2$ [Prakash et al., 1992]. The uncorrelated case corresponds to $\lambda = 0$. The fractal dimension of the infinite cluster remains equal to that of the classical percolation infinite cluster, i.e., $d_f = 1.896$. The fractal dimension of the backbone, however, increases with increasing correlation and becomes equal to the infinite cluster fractal dimension when $\lambda \rightarrow 2$. Thus the backbone becomes increasingly compact as λ increases. The anomalous diffusion exponent is directly computed and found to vary in the range [2.29, 2.878] for $\lambda \in [0, 1.75]$ [Prakash et al., 1992]. The dispersion of the exponent values is very limited.

[35] Comparison between continuum and correlated percolations shows that for continuum percolation, diffusion is slowed down by the increase in heterogeneity when compared to the classical percolation theory case ($d_w \geq 2.878$), whereas for correlated percolation, structures are more compact and diffusion is sped up ($d_w \leq 2.878$). A structure

cumulating correlations and permeability distribution has been studied based on a truncated fractional Brownian motion (fBm) [Sahimi and Mukhopadhyay, 1996]. A three-dimensional fBm is first generated and the permeability values are proportional to its two-dimensional projection. The smallest permeabilities are removed until the percolation threshold is reached. The fBm is parameterized by the Hurst exponent $H \in [0, 1]$ leading to highly correlated structures persistent for $H > 0.5$ and nonpersistent for $H < 0.5$. For $H = 0.2$ and 0.8 , permeability values are distributed over 1 and 2 orders of magnitude, respectively. The resulting structure is not stationary and its correlations are different from that of Prakash *et al.* [1992]. In fact, the Fourier power spectrum of the truncated fBm and correlated percolation are power laws of characteristic exponents equal to $-(2 + 2H) \in [-4, -2]$ and to $-\lambda \in [-2, 0]$, respectively. Close results are found on the infinite cluster and backbone fractal dimensions. The fractal dimension of the infinite cluster is difficult to compute exactly between its classical values of 1.896 and 2. The backbone fractal dimension gradually increases to the infinite cluster dimension, showing that the structures become increasingly compact. The anomalous diffusion exponent is obtained from the permeability scaling exponent $\tilde{\mu}$ by Einstein's relation (7). d_w spans a narrow range [2.73, 2.878], which could be due to the counteracting effects of the correlation and permeability distribution previously underlined in the comparison between the two cases of continuum and correlated percolations.

4.3. Discussion

[36] Whatever the structure (Sierpinski- or percolation-like), d_w and n can be defined over the whole time range. The range of exponent values from the percolation structure is narrower than that from the Sierpinskis, reflecting their smaller diversity in terms of fractal dimension. In fact, the fractal dimension of percolation-like structures is restricted to their values obtained for the backbone and the infinite cluster.

[37] The anomalous diffusion exponents d_w of Sierpinski-like structures are contained in the range [1.9, 2.5], whereas most of the d_w values for percolation-like structures are larger than 2.878, except for more compact correlated percolation structures. Sierpinski and percolation structures are in fact geometrically very different. The salient feature of Sierpinskis is the presence of holes at all scales, whereas flow in percolation structures is controlled by critical bonds that are the singly connected red bonds in classical percolation and that generalize to bonds of very low permeability in continuum percolation [Charlaix *et al.*, 1987]. Critical links acting as bottlenecks thus induce a more anomalous transport than holes.

[38] As regards percolation and Sierpinski-like structures, d_w values between 1.9 and 2.5 are indicative of a Sierpinski-like structure, whereas d_w values larger than 2.86 rather reveal a percolation-like structure. Different structures can explain d_w values larger than 2.86. The first one is the permeability heterogeneity of the structure as in the typical case of continuum percolation. The second one is an increase in the density of critical bonds. For example, the extreme case of the Péano curve, for which all links are critical, has an anomalous diffusion exponent $d_w = 4$ in two dimensions. The third one is an increase in the Euclidean

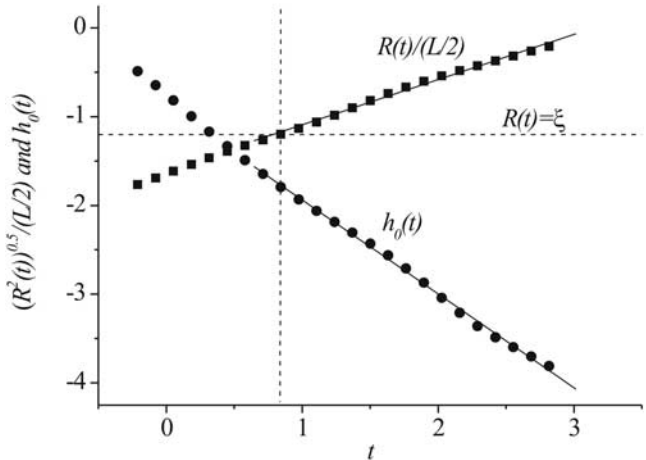


Figure 6. Square root of R^2 normalized by half the system size ($L/2$) and h_0 against time in a bi-logarithmic graph for an exponentially correlated lognormal random field. The correlation length ξ is equal to $1/32$ of the system size L , $L = 256$, and the lognormal variance is 3. R^2 and h_0 have been fitted by linear functions ($R^2(t) \sim t$ and $h_0(t) \sim 1/t$) in the time range for which the radius of diffusion is larger than the correlation length ξ . The time range begins at the dashed vertical line. By calculating directly d_w on 100 realizations for a lognormal variance of 2, we found that the average value of d_w is 2.1, in fact close to 2, and the standard deviation of the d_w values remains limited to 0.15.

dimension. In three dimensions, the Sierpinski gasket and the percolation infinite cluster have anomalous diffusion exponents equal to 2.58 and 3.8, respectively, which are in fact larger than their two-dimensional counterparts 2.322 and 2.878, respectively.

[39] For all structures except the Sierpinski lattices, the hydraulic dimension n can be notably different from the fractal dimension, as shown by equations (5) and (11). The flow dimension can be derived from the anomalous diffusion exponent d_w and the fractal dimension d_f by equation (5). For Sierpinski lattices, d_w and n are found to depend both on the general fractal dimension d_f and on local conditions that are adequately quantified by the order of the injection link. As a consequence, relation (5) between d_f , d_w , and n does not hold and is replaced by relation (11) relating exponents n and d_w to exponent d_N . d_N represents the scaling of the mass from the injection point.

5. Flow and Anomalous Diffusion Exponents in Continuous Heterogeneous Media

[40] Fractal media are the first types of media studied for fractional flow because of their scale-dependent geometrical structure. From the same idea, continuous media could induce a fractional flow signal provided that their permeability field displays scale-dependent correlations. First, we verify that classically lognormally correlated media do not induce any fractional flow. In fact, the drawdown observations are found to be well accounted for by the classical interpretation framework of Theis in two dimensions [Meier *et al.*, 1998; Walker and Roberts, 2003]. This is confirmed by the numerical results of Figure 6 showing that linear fitting of $R^2(t)$ and $h_0(t)$ leads to a good representation.

[41] Second, we look at long-range correlated media. The anomalous diffusion exponent d_w is computed on systems for which correlations are generated by a fractional Brownian motion [Saadatfar and Sahimi, 2002]. Like in the correlated percolation case, the fractional Brownian motion is generated in three dimensions and is projected in the two-dimensional plane. It is characterized by the Hurst exponent H . When the permeability field K follows the fBm statistics, d_w remains equal to 2 whatever H [Saadatfar and Sahimi, 2002]. However, when the logarithm of K follows the fBm statistics ($\ln K$ fBm), diffusion is normal when $H > 0.5$ and anomalously slow when $H \leq 0.5$. When $H > 0.5$, the highest permeability values form a compact structure dominating diffusion and inducing a normal diffusion. When $H \leq 0.5$, $d_w = 2.45, 2.25$, and 2.06 for $H = 0.1, 0.3$, and 0.5 , respectively [Saadatfar and Sahimi, 2002]. Anomalous diffusion is due to the presence of islands of very low permeability that slow down diffusion. This is consistent with the note on the difficulty of fitting a Theis model for a $\ln K$ fBm with $H = 0.25$ by Meier *et al.* [1998]. For $H = 0.25$, Walker *et al.* [2006] found a mean exponent n of 2 but a large standard deviation increasing with time, which could explain their slightly different result for the mean of n . Addition of large anisotropy to $\ln K$ fBm removes the anomalous diffusion in the direction perpendicular to the medium stratification [Saadatfar and Sahimi, 2002]. Finally, the deletion of 10% of the lowest permeability induces log-periodic oscillations in time of the exponent value, thus impeding a consistent exponent definition. Similar oscillations are also observed in Sierpinski carpets and are attributed to the existence of holes within the medium acting as “internal boundaries” [Sellers and Barker, 2005]. As particles move away from the boundaries, they speed up until they are influenced by another internal boundary.

[42] Other continuous long-range correlation systems are “continuous” multifractals having a support of fractal dimension (i.e., the zeroth-order dimension) equal to the embedding Euclidean dimension. d_w and n are computed on “continuous” multifractals generated by a multiplicative cascade process parameterized by the correlation dimension (second-order dimension) D_2 ($1 \leq D_2 \leq 2$) [de Drezy *et al.*, 2004]. The Fourier spectrum of these structures is a power law of slope $-D_2 \in [-2, -1]$ larger than that of the previous fBm equal to $-(2 + 2H) \in [-4, -2]$. Long-range correlations are thus less present in multifractals than in fBms. For such media, the anomalous diffusion exponent d_w and the hydraulic dimension n averaged over a large number of realizations are always equal to 2 whatever the correlation dimension D_2 . However, the exponent variability is large, as d_w values range from 0.5 to 3. d_w and n strongly depend on a local property, i.e., the permeability at the injection point K_{in} . In fact, because of the long-range correlations, the permeability at the injection point is linked to the permeability scaling of $K(r) \sim r^{-\theta_0}$ and through it to exponent d_w leading to:

$$d_w = 4 - D_2 + \theta_0 \text{ with } \theta_0 = \frac{\log_{10} (K_{\text{unit}}/K_{\text{in}})}{\log_{10} (l_{\text{min}}/L)}, \quad (12)$$

where K_{unit} and l_{min} are the permeability and length references, respectively [de Drezy *et al.*, 2004]. The

hydraulic dimension is given by relation (5). These results underline three points. First, depending on the permeability scaling from the well, diffusion can be either anomalously slow ($d_w > 2$) or anomalously fast ($d_w < 2$). For a given configuration, diffusion may be anomalously fast and d_w values lower than 2 can be found. Second, when $d_w < 2$, the hydraulic dimension n is larger than the Euclidean dimension 2, showing again the difference between the hydraulic dimension and the fractal dimension (here equal to 2). The hydraulic exponents n and d_w depend on a local as well as on a global characteristic, i.e., the permeability at the injection point and the correlation dimension, respectively. Expressing n and d_w as a function of D_2 and K_{in} yields a standard deviation of n and d_w around 0.4, which is twice smaller than when expressing n and d_w as a sole function of D_2 .

[43] By comparing the exponents of these different structures, we conclude that long-range correlated continuous permeability fields can induce anomalous diffusion behaviors as long as they are not too much correlated, more precisely, if the power law exponent of their Fourier spectrum is larger than -2.

6. Discussion

[44] In sections 4 and 5, we have obtained exponents n and d_w on fractal and continuous multifractal structures. It is a kind of direct problem for the transient flow equation. The corresponding inverse problem consists in deriving geometrical and hydraulic structures from n and d_w values. The inverse problem is typically posed in field studies where nontrivial n and d_w values are observed. These values cannot be directly used to specify a larger model or to make predictions with other well configurations. The underlying geometrical and hydraulic information could however be used. The comparison between n and d_w field data and numerical or theoretical values should account for the field specificities. First, a given field corresponds to a single realization and second, well tests are generally performed from a unique well location. These specificities are echoed in the numerical results of sections 4 and 5. n and d_w can be quite different in two different realizations with the same fixed parameters, and n and d_w are sensitive to the location of the well within the structure. Field data should thus be compared to single realization values rather than to averages. The exponent variability appears to be as important as the mean tendency.

[45] We display in the (n, d_w) graphs of Figures 7a and 7b the exponent coverage obtained for the range of fractal and continuous multifractals studied in sections 4 and 5. The variability is calculated for most Sierpinski and continuous multifractals. The realization-based values found for Sierpinski, percolation-like, and continuous structures cover large zones in the (n, d_w) graph. For percolation-like structures, average (n, d_w) data are clustered around the curve $d_w = 3.9/n$. For Sierpinski structures, average (n, d_w) data cover a large band below $d_w = 2.5$. For continuous multifractals, values obtained on a realization basis lie between the two thin dashed lines, the mean value being represented by the thin black line. Because of the large exponent variability (around 0.8) due to the large range of possible permeability scalings from the well, continuous multifractals cover most of the (n, d_w) plane. When com-

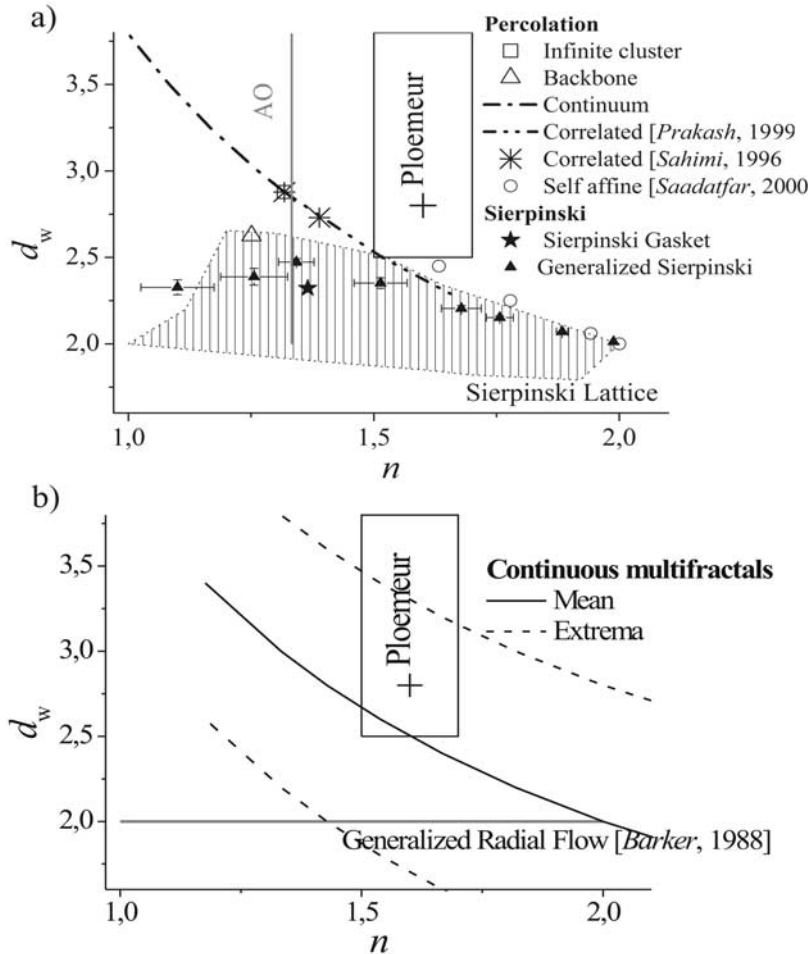


Figure 7. Diagram $n-d_w$ for the different structures using the Ploemeur data. The cross is placed at the most probable value and the embedding rectangle stands for the imprecision. “AO conjecture” is the abbreviation for the Alexander and Orbach conjecture.

pared to a realization basis, almost all (n, d_w) data could be modeled by continuous multifractals.

[46] We compare these results to the Ploemeur field data obtained from a test performed at a given well. Figure 7 shows the most probable exponent value obtained in Ploemeur ($n = 1.5$, $d_w = 2.8$) and the uncertainty (thin rectangle). None of the studied two-dimensional fractal structures is relevant for the site of Ploemeur (Figure 7a). The only overlap among the presented models concerns the continuous multifractal (Figure 7b). We characterize more precisely the multifractals consistent with the most probable value $d_w = 2.8$. Equation (12) leads to the following relation between D_2 and θ_0 : $4 - D_2 + \theta_0 = 2.8$. From a unique well test, the global parameter (D_2) and the local one (θ_0) cannot be separated. The global characteristic D_2 could be extracted from the local characteristic θ_0 by performing several well tests from different wells as well as observations on distant piezometers. The comparison based on averages is much more selective in terms of model. However, extracting average (n, d_w) values from field data requires performing well tests from different wells and observing drawdowns on distant piezometers.

[47] On the basis of the available data, continuous multifractals may not be the only model able to fit the Ploemeur

data. Other heterogeneity types leading to the same range of (n, d_w) values should have, on average, large d_w values while keeping n values between 1.5 and 2. Three-dimensional structures would give large d_w and d_f values leading to n values below 2 as for example ($n = 1.55$, $d_w = 2.58$) for the three-dimensional Sierpinski gasket and ($n = 1.33$, $d_w = 3.8$) for the three-dimensional percolation cluster. Note, however, that we are not necessarily wide of the mark with two-dimensional structures since a great number of aquifers are thin layers that could be assimilated to two-dimensional plane. In Ploemeur, from which the hydraulic exponents have been carefully derived, the main flow zone is a contact zone between a granitic pluton and a micaschist formation. This is the reason why we make the comparison between the Ploemeur results and this study, although we acknowledge for possible three-dimensional effects that would make the comparison irrelevant.

[48] This study addresses an important issue to interpret field data, which is the contribution of local effects that makes single realization-based scaling exponents different from their average value. Indeed, as for most of natural data, the well tests performed in Ploemeur have all been performed from the same well. The results obtained from the continuous multifractals emphasize the contribution of local

effects that lead to large range of (n , d_w) values. Displaying only average values of the synthetic exponents would have led to the erroneous interpretation of an absence of overlap.

7. Conclusion

[49] Originally, fractional flow models have been expressed as generalized differential flow equations depending on two exponents: the hydraulic dimension n and the anomalous diffusion exponent d_w . Beyond the consistency of these equations and the anomalous drawdown signals, the underlying heterogeneity is barely known. Because fractional flow models are intrinsically scaling models, we tested two kinds of scaling media: fractals and continuous long-ranged correlated continuous media. These media display anomalous behaviors consistent with those postulated by fractional flow models, i.e., a hydraulic dimension n different from the integers 1, 2, and 3, and an anomalous diffusion exponent d_w different from 2. First, we note that the hydraulic dimension is notably different from the fractal dimension as also shown by relation (5). Second, for fractals, the anomalous diffusion exponent d_w of Sierpinski structures are in the range [2, 2.5], whereas for the percolation cluster at threshold, they are generally larger than 2.8. The bottlenecks typical of the percolation cluster induce higher slowdowns than the holes typical of Sierpinski. Third, for Sierpinski lattices (Figure 2d) and multifractal continuous structures, exponents n and d_w are conditioned both by the fractal and correlation dimensions and by some local properties of the structure around the injection point. Because n and d_w depend on local properties, we propose first to derive them on several points of the field and second to obtain their underlying average characteristic, being in this case the fractal dimension or the correlation dimension.

References

- Acuna, J. A., and Y. C. Yortsos (1995), Application of fractal geometry to the study of networks of fractures and their pressure transient, *Water Resour. Res.*, **31**, 527–540.
- Acuna, J. A., I. Ershaghi, and Y. C. Yortsos (1992), Practical applications of fractal pressure transient analysis of naturally fractured reservoirs, SPE 24075 presented at the 1992 SPE Annual Fall Meeting, Soc. of Pet. Eng., Washington, D. C.
- Alexander, S., and R. Orbach (1982), Density of states of fractals: ‘Fractons’, *J. Phys. Paris*, **43**, L625–L631.
- Bangoy, L. M., P. Bidaux, C. Drogue, R. Plégat, and S. Pistre (1992), A new method of characterizing fissured media by pumping tests with observation wells, *J. Hydrol.*, **138**, 77–88.
- Barker, J. A. (1988), A generalized radial flow model for hydraulic test in fractured rock, *Water Resour. Res.*, **24**, 1796–1804.
- Berkowitz, B., and I. Balberg (1993), Percolation theory and its application to groundwater hydrology, *Water Resour. Res.*, **29**, 775–794.
- Charlaix, E., E. Guyon, and S. Roux (1987), Permeability of a random array of fractures of widely varying apertures, *Transp. Porous Media*, **2**, 31–43.
- Dasgupta, R., T. K. Ballabh, and S. Tarafdar (1999), Scaling exponents for random walks on Sierpinski carpets and number of distinct sites visited: A new algorithm for infinite fractal lattices, *J. Phys. A Math. Gen.*, **32**, 6503–6516.
- de Dreuzy, J.-R., P. Davy, J. Erhel, and J. de Brémont d’Ars (2004), Anomalous diffusion exponents in continuous 2D multifractal media, *Phys. Rev. E*, **70**.
- Doughty, C., and K. Karasaki (2002), Flow and transport in hierarchically fractured rock, *J. Hydrol.*, **263**, 1–22.
- Feder, J. (1988), *Fractals*, Springer, New York.
- Grassberger, P. (1999), Conductivity exponent and backbone dimension in 2-D percolation, *Physica A*, **262**, 251–263.
- Hamm, S.-Y., and P. Bidaux (1996), Dual-porosity fractal models for transient flow analysis in fissured rocks, *Water Resour. Res.*, **32**, 2733–2745.
- Havlin, S., and D. Ben-Avraham (1987), Diffusion in disordered media, *Adv. Phys.*, **36**, 695–798.
- Hindmarsh, A. C. (1983), Odepack, a systematized collection of ODE solvers, in *Scientific Computing*, edited by R. S. Stepleman et al., pp. 55–64, IMACS/North-Holland Publishing Company, Amsterdam.
- Kim, M. H., D. H. Yoon, and I. M. Kim (1993), Lower and upper-bounds for the anomalous diffusion exponent on Sierpinski carpets, *J. Phys. A Math. Gen.*, **26**, 5655–5660.
- Kogut, P. M., and J. P. Straley (1979), Distribution-induced non-universality of the percolation conductivity exponent, *J. Phys. C Solid State Phys.*, **12**, 2151–2159.
- Kuusela-Lahtinen, A., A. Niemi, and A. Luukkonen (2003), Flow dimension as an indicator of hydraulic behavior in site characterization of fractured rock, *Ground Water*, **41**, 333–341.
- Le Borgne, T., O. Bour, J.-R. de Dreuzy, P. Davy, and F. Touchard (2004), Equivalent mean flow models for fractured aquifers: Insights from a pumping tests scaling interpretation, *Water Resour. Res.*, **40**, W03512, doi:10.1029/2003WR002436.
- Leveinen, J. (2000), Composite model with fractional flow dimensions for well test analysis in fractured rocks, *J. Hydrol.*, **234**, 116–141.
- Matcha, J., R. A. Guyer, and S. M. Moore (1986), Conductivity in percolation networks with broad distributions of resistances, *Phys. Rev. B*, **33**, 4818–4825.
- Meier, P. M., J. Carrera, and X. Sánchez-Villa (1998), An evaluation of Jacob’s method for the interpretation of pumping tests in heterogeneous formations, *Water Resour. Res.*, **34**, 1011–1025.
- O’Shaughnessy, B., and I. Procaccia (1985), Diffusion on fractals, *Phys. Rev. A*, **32**, 3073–3083.
- Porto, M., A. Bunde, S. Havlin, and H. Roman (1997), Structural and dynamical properties of the percolation backbone in two and three dimensions, *Phys. Rev. E*, **56**.
- Prakash, S., S. Havlin, M. Schwartz, and H. E. Stanley (1992), Structural and dynamical properties of long-ranged correlated percolation, *Phys. Rev. A*, **46**, R1724–R1727.
- Riemann, K., G. V. Tonner, and P. Dzanga (2002), Interpretation of single-well tracer tests using fractional-flow dimensions. Part 2: A case study, *Hydrogeol. J.*, **10**, 357–367.
- Roman, H. E. (2004), How does the diffusion equation on fractals look?, *Fractals*, **12**, 149–156.
- Saadatfar, M., and M. Sahimi (2002), Diffusion in disordered media with long-range correlations: Anomalous, Fickian, and superdiffusive transport and log-periodic oscillations, *Phys. Rev. E*, **65**, 036116.
- Sahimi, M. (1996), Linear and nonlinear, scalar and vector transport processes in heterogeneous media: Fractals, percolation, and scaling laws, *Chem. Eng. J. Biochem. Eng. J.*, **64**, 21–44.
- Sahimi, M., and S. Mukhopadhyay (1996), Scaling properties of a percolation model with long-ranged correlations, *Phys. Rev. E*, **54**, 3870–3880.
- Sellers, S., and J. A. Barker (2005), Anomalous diffusion in simulations of pumping tests on fractal lattices, in *Understanding the micro to macro behaviour of rock-fluid systems*, edited by R. P. Shaw, Geological Society, London, Special Publications **249**, 79–89 pp.
- Stauffer, D., and A. Aharony (1992), *Introduction to percolation theory*, 2nd ed., Taylor and Francis, Philadelphia, Pa.
- Stenull, O., and H.-K. Janssen (2001), Conductivity of continuum percolating systems, *Phys. Rev. E*, **64**, doi:10.1103/PhysRevE.64.056105.
- Theis, C. V. (1935), The relation between the lowering of the piezometric surface and the rate and duration of discharge of a well using groundwater storage, *Eos Trans. AGU*, **16**, 519–524.
- Walker, D. D., and R. M. Roberts (2003), Flow dimensions corresponding to hydrogeologic conditions, *Water Resour. Res.*, **39**(12), 1349, doi:10.1029/2002WR001511.
- Walker, D. D., P. A. Cello, A. J. Valocchi, B. Loftis (2006), Flow dimensions corresponding to stochastic models of heterogeneous aquifers, *Geophys. Res. Lett.*, **33**, L07407, doi:10.1029/2006GL025695.

P. Davy and J.-R. de Dreuzy, Géosciences Rennes, UMR 6118 CNRS, Université de Rennes, Campus de Beaulieu, F-35042, Rennes Cedex, France. (jean-raynald.de-dreuzy@univ-rennes1.fr)